Influence of spatial exclusion on the statistical behavior of attached eddies

Charitha M. de Silva,[*] James D. Woodcock, Nicholas Hutchins, and Ivan Marusic
Department of Mechanical Engineering, University of Melbourne, Victoria 3010, Australia

Recent studies have shown Townsend's attached eddy hypothesis to be a promising basis for modeling the velocity statistics in the logarithmic region of turbulent wall flows. Accordingly, the attached eddy model is able to reliably estimate the functional forms of the mean velocity, second-order moments of the velocity fluctuations, and recently structure functions and higher-order moments of the velocity fluctuations. However, detailed quantitative comparisons with experimental results reveal differences, particularly for the higher-order moments. Specifically, the predicted flatness (kurtosis) is found to be invariably greater than 3 (i.e., super-Gaussian behavior) for all velocity components, while experimental results show sub-Gaussian behavior for the streamwise component of velocity. In this study, we show that this and other discrepancies can be resolved by considering the finite space occupied by each eddy. Earlier models had allowed each eddy to be perfectly randomly located, with no consideration for the locations of neighboring eddies (in other words, their locations can be described as a Poisson point process). Here we investigate the effect of mandating a minimum distance between any two eddies of the same height. We demonstrate that this spatial exclusion, when combined with an experimentally observed shape for the representative eddy, produces predictions that are now in better agreement with experimental observations. In particular, sub-Gaussian behavior is now attained for the streamwise component, while super-Gaussian behavior is maintained for the other velocity components, qualitatively matching experimental findings. Therefore, our findings infer that spatial exclusion between eddies is likely to play an important role in the laws that govern their spatial arrangement, which is likely to be more disperse than a Poisson point process.

I. INTRODUCTION

Because of its inherent complexity, turbulence is notoriously resistant to attempts at physical modeling. The greatest impediment to developing physical models is that turbulent flows consist of motions on a multitude of scales, all of which interact, and all must therefore be accounted for within a model. However, in the so-called logarithmic region of turbulent wall flows, the energy-containing scales of motion may now be modeled via the attached eddy hypothesis. The hypothesis, which was first proposed by Townsend [1] and extended by Perry and Chong [2], states that the flow can be represented by a hierarchy of geometrically self-similar flow patterns (or eddies), which extend from the wall into the flow. Modeling of turbulent flows, based upon this hypothesis, has been found to reproduce many of the statistical features of real turbulent flows.

Recently, Woodcock and Marusic [3] placed the attached eddy hypothesis on a more rigorous physical and mathematical footing. Their work also derived the higher-order moments of the velocity fluctuations, and it was here that the limitations of the present model became apparent. While the first- and second-order moments have shown good qualitative agreement with experimental results, a clear difference emerges at the fourth order: While experimental flows show the streamwise velocity to have a flatness of around 2.8 [4], the model predicts that the streamwise flatness will invariably be greater than 3. Addressing this discrepancy is the subject of this work.

---

[*]Corresponding author: desilvac@unimelb.edu.au

Until now, models based upon the attached eddy hypothesis have assumed that the eddies are perfectly randomly and independently located in the plane of the wall. In mathematical terminology, the placement of the eddies on the wall would be described as a Poisson point process (often simply referred to as a Poisson process) and the location of each individual eddy follows a uniform distribution. However, while this is a suitable distribution for simple points on a plane, it has obvious drawbacks when applied to eddies that inhabit a finite region of space. Notably, it allows two or more eddies to overlap with no restriction. In reality though, perfectly overlapping eddies would result in excessively large localized velocity gradients leading to a possible scenario where vortex cores would overlap. In addition, eddies in close proximity would have overlapping velocity fields that would mutually interact (to be detailed further). It is likely, therefore, that real eddies do not always encroach upon their neighbor's space and their spacing will therefore be more dispersed than a Poisson process.

In this Rapid Communication we examine the influence of eddy placement on flow statistics computed from synthetic velocity fields based on the attached-eddy model (AEM). Emphasis is placed on the flatness since prior work has shown that eddies arranged in a Poisson process fail to correctly predict empirical findings from experiments. Since the flatness is a measure of the extent to which the standard deviation results from larger deviations from the mean, an increased separation between closely located eddies would be expected to reduce the flatness. Again, the extent of this reduction will depend upon the shape of the velocity field associated with the representative eddy. This will be discussed further when we present our results.

Throughout this work x, y, and z refer to the streamwise, spanwise, and wall-normal directions, respectively. The corresponding instantaneous streamwise, spanwise, and wall-normal velocity fluctuations are represented by u, v, and w. Overbars indicate averaged quantities and the superscript and subscript $+$ refer to normalization by inner scales. For example, we use $l^+ = lU_\tau/\nu$ for length and $u^+ = u/U_\tau$ for velocity, where U_τ is the mean friction velocity and ν is the kinematic viscosity of the fluid.

II. SPATIAL EXCLUSION AND THE ATTACHED EDDY MODEL

From the conception of the attached eddy model until now the placement of representative eddies was considered to be independent [1]. Instead, to influence the degree of dispersion between eddies, we consider a system in which the placement is not entirely independent by mandating a minimum separation μ between any two eddies of the same size. In the present analysis for each hierarchical eddy μ is expressed as

$$\mu = \frac{A_o}{A_e},\tag{1}$$

where A_o corresponds to an exclusion zone (or area) around the center of an eddy and A_e equals the rectangular spatial extent or footprint of a representative eddy at the wall [Fig. 1(a)]. We note the parameter μ is used as a tool or measure that controls the degree of overlap between eddies. Hence, a simplified rectangular footprint is employed. Further, the exclusion zone around each eddy applies only to other eddies of the same size (or hierarchical length scale). Conversely, eddies from different sizes are still placed independently, which causes eddies of different sizes to overlap at the same degree of a Poisson process. As a consequence, smaller eddies may reside beneath or within the footprint of larger eddies (see Fig. 1). Such an arrangement concurs with empirical observations and existing theoretical models, which have hypothesized that small eddies may nestle within larger eddies, and this appears to be more prevalent at higher scale separation [1,2,5–8]. Such a structural composition would not be possible if the eddies were not allowed to overlap at different sizes.

The described spatial arrangement of eddies and the influence of μ is illustrated in Figs. 1(b) and 1(c). The first example in Fig. 1(b) has no exclusion zone (i.e., $\mu = 0$), therefore, the placement of eddies follows a Poisson process where adjacent eddies are free to overlap (red hatched regions). Figure 1(c) illustrates an example where $\mu = 0.5$, therefore the average overlap between adjacent
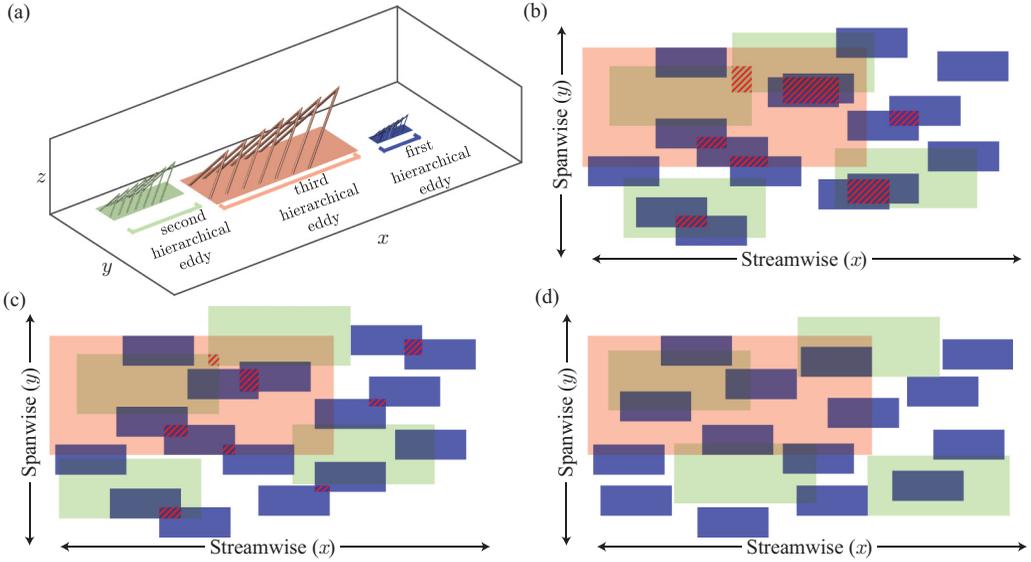
FIG. 1. (a) Schematic of the spatial footprint of typical representative Λ packet eddies for three hierarchical eddies (pink, green, and blue). (b) Example where eddy placement at each hierarchical length scale is not influenced by spatial exclusion (Poisson point process, $\mu = 0$). (c) Exclusion zone equaling approximately half the eddy size ($\mu \approx 0.5$). (d) Exclusion zone larger than the size of the eddy ($\mu > 1$). The red hatched patches in (b)–(d) indicate overlapping regions between eddies of the same hierarchical length scale.

eddies is lower (fewer highlighted regions). If we further restrict the overlap so that $\mu > 1$, there will be no overlap between eddies of the same size, which is shown in Fig. 1(d).

In the present study, following recent work [3,9,10], we employ a representative packet eddy consisting of seven Λ eddies (see Fig. 2). Each eddy within the packet has an average eddy spacing of 0.4ℓ (where ℓ is the wall-normal height of the largest eddy in the packet) and an inclination angle $\alpha = 10°$. We note that prior work has shown that flow statistics computed employing a similar
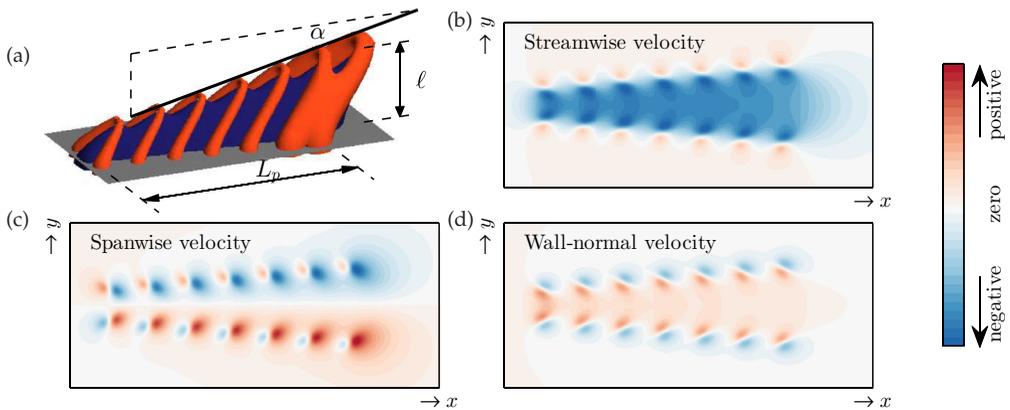
FIG. 2. (a) Schematic of a typical representative Λ packet eddy, adapted from [9]. The blue region isolates the low-momentum region that forms beneath the train of Λ eddies and the red region corresponds to a higher-speed region. Color contours of (b) streamwise, (c) spanwise, and (d) wall-normal velocity contributions from the Λ packet eddy shown in (a). Contour levels are equal for all three velocity components in (b)–(d) and are computed on the wall-parallel plane highlighted in gray in (a) at $z = 0.1\ell$.

representative packet eddy are in good agreement for the logarithmic-law constants and Reynolds stresses [3,10]. Additionally, recent work has also revealed similarities in the structural organisation between AEM synthetic velocity fields and experimental work [9], therefore, we believe the chosen representative eddy forms a good baseline for the present case.

The velocity fields for u, v, and w from the chosen representative packet eddy are shown in Figs. 2(b)–2(d) from a wall-parallel slice at $z = 0.1\ell$. It must be stressed here that the shape of the representative eddy has not been chosen in order to produce a particular statistical behavior or satisfy a particular outcome. Instead, the representative eddy shape used in both the present and prior work using the attached-eddy model follows preceding evidence of the structural composition of boundary layers from both experimental and numerical works [5,11,12]. These include, for example, large streamwise elongated structures observed in the logarithmic region [13] and regions of uniform streamwise momentum [9,14].

To compute each synthetic velocity field, Biot-Savart calculations are performed for a single representative Λ eddy. A Gaussian distribution of vorticity is assumed in the cores of the vortices or rods that constitute each Λ eddy [15]. This process is then repeated for each eddy within a packet and at different hierarchical length scales. The representative length scales follow a geometric pattern, which can be exploited to minimize computational time due to the self-similarity between flow fields at different length scales in the overall hierarchy. The spatial population density (and domain size) is held constant and chosen such that the mean streamwise velocity profile in the logarithmic region satisfies the logarithmic-law constants. More extensive details on the computational process to generate the synthetic databases and scaling of the velocity fields can be found in Ref. [9]. It is worth highlighting that we have not attempted to match all the mean flow and Reynolds stresses from the synthetic data sets. Instead, our focus here is on the effect of adding a minimum exclusion between what would otherwise be a random and independent distribution of eddies.

For the present study, synthetic volumetric velocity fields are generated at a fixed Reynolds number of $\mathrm{Re}_\tau = 6400$, chosen to be sufficiently high to clearly observe a logarithmic region but still at manageable computational cost. Following Perry and Marusic, we fix the smallest packet-eddy length scale to be on the order of $100\nu/U_\tau$ (following the Kline *et al.* [16] scaling), after which the number of hierarchical packet eddies N_{h} follows a geometric progression. The spatial resolution (or grid spacing) of the velocity fields is fixed at 15 viscous units, closely resembling prior work using AEM synthetic data sets [3,9]. Additionally, this ensures that the smallest representative eddies of $\mathcal{O}(100^+)$ are sufficiently resolved. An in-depth analysis of these parameters can be found in Ref. [9]. To investigate the influence of the spatial exclusion zone μ, AEM synthetic data sets are computed for $\mu = 0.25$, 0.5, 0.75, and 1. To ensure a sufficient degree of convergence, each data set consists of 5000 independent volumes. Although not reproduced here for brevity, the degree of convergence up to the sixth-order moment was verified following an approach outlined by Meneveau and Marusic [17].

Analysis of velocity statistics

Next we use the synthetic AEM velocity fields to examine statistical properties of the flow, now with a specified separation between eddies of the same scale μ following Eq. (1). It is important to note that results are only presented in the range $0 \leqslant \mu \leqslant 1$. A further increase in μ would necessitate a larger streamwise and spanwise spatial domain in order to ensure adequate space to place all the eddies. However, our domain size is fixed to satisfy empirically observed constants in the mean flow (see Ref. [9] for further details).

Figure 3 presents the turbulence intensity for the three velocity components as a function of μ. The results show that increasing μ has the effect of decreasing $\overline{u^2}$, and to a lesser extent $\overline{v^2}$, while having a negligible effect on $\overline{w^2}$, indicating that the presence of a spatial exclusion zone around each eddy has largely reduced the variance. This observation is likely caused by constructive interference between velocity fields of two overlapping eddies, which is particularly evident for the streamwise velocity. Such a scenario is illustrated in Fig. 4, which shows the magnitudes of the streamwise and
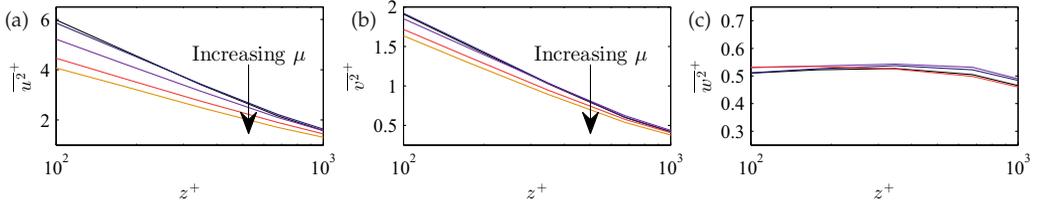
FIG. 3. Second-order velocity moments for the (a) streamwise, (b) spanwise, and (c) wall-normal velocity components verses z^+. The superscript $+$ denotes normalization by inner scales. Each solid line is computed at different spatial exclusions in the range $\mu = 0$–1, with the darkest shading (black) corresponding to $\mu = 0$.
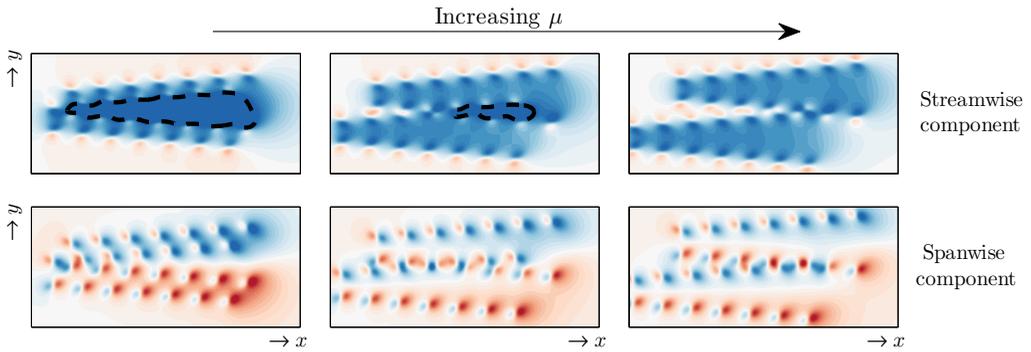
FIG. 4. Color contours of streamwise (top row) and spanwise (bottom row) velocity contributions from two randomly placed representative eddies of the same hierarchical length scale. Velocity fields are shown on the wall-parallel plane highlighted in gray in Fig. 2(a) at $z = 0.1\ell$ and the color contour levels match Fig. 2. Each vertical column represents different magnitudes of the spatial exclusion parameter μ, which increases from left to right. The black dashed lines encapsulate strong negative streamwise velocity contributions mainly residing in the overlap region of the eddies.
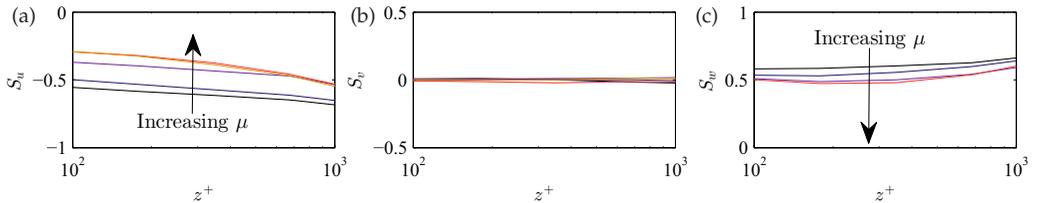
FIG. 5. Skewness for the (a) streamwise, (b) spanwise, and (c) wall-normal velocity components verses z^+. Color representation as in Fig. 3.
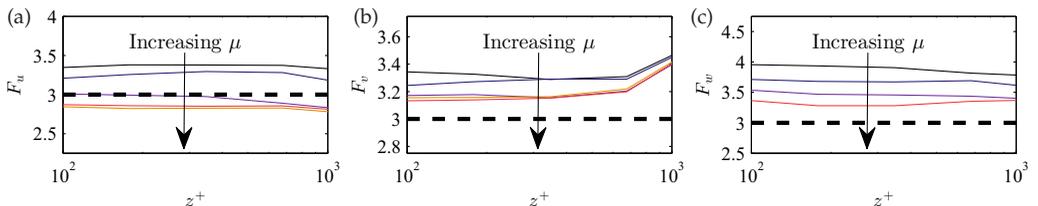
FIG. 6. Flatness for the (a) streamwise, (b) spanwise, and (c) wall-normal velocity components verses z^+. Color representation as in Fig. 3 and the dashed line corresponds to a flatness of 3, which demarcates sub-Gaussian behavior.
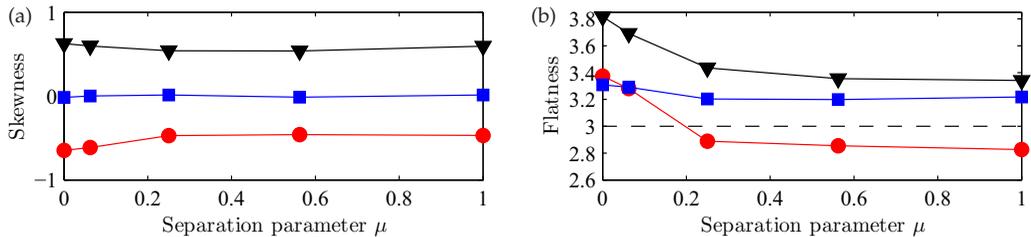
FIG. 7. (a) Skewness and (b) flatness as a function of spatial exclusion parameter μ. Results are presented at the geometric center of the logarithmic region at $\mathrm{Re}_\tau = 6400$. The symbols ●, ■, and ▼ correspond to the streamwise, spanwise, and wall-normal velocity components, respectively.

spanwise velocities at different μ. The dashed lines overlaid on contours of streamwise velocity at lower μ show the dominant constructive interference regions, where the streamwise velocity exhibits a large negative flow through the legs of each eddy in the packet. Because of this, if two eddies encroach upon each other, their velocity fields will largely add together, significantly increasing their combined contribution to $\overline{u^2}$. By contrast, unless the two eddies are almost colocated, their spanwise velocity fields will not constructively interfere. Hence, the effect of separating the eddies is greatest in the streamwise direction, which is borne out in our results. We note that the behavior of the w component is similar to the spanwise component and is therefore not reproduced here for brevity [Figs. 2(c) and 2(d) show the qualitative similarity between spanwise and wall-normal components].

A similar effect is observed for the skewness (computed following $S_u = \overline{u^3}/\overline{u^2}^{3/2}$ for the streamwise component), which is shown in Fig. 5. The results show that the magnitude of the streamwise and wall-normal skewnesses both decrease as μ increases (note that S_u is always negative). These observations can also be explained by the increasing separation between eddies at larger μ, since any closely located eddies will greatly contribute to the skewness. The spanwise skewness that is nominally zero at $\mu = 0$ remains unaffected by μ.

Figure 6 shows results for the flatness, which is defined such that $F_u = \overline{u^4}/\overline{u^2}^2$ for all three velocity components. The results show that at $\mu = 0$ the flatness is greater than 3 in all directions and decreases with higher μ. However, the crucial result here is that F_u decreases fastest and is the only component to show sub-Gaussian behavior with a magnitude below 3. This behavior is likely to be caused by a combination of the eddies' distribution (the influence of μ) and their shape (illustrated in Fig. 4 and detailed in the preceding discussion). Furthermore, we can see in Fig. 7 that increasing μ has a diminishing effect on the flatness. In any case, one would not expect to have a μ much greater than 1, which implies that the excluded zone around each eddy reaches beyond the coherent structure itself (the high-vorticity region depicted in Fig. 2).

As a final note, the nearly asymptotic magnitude of $F_u \simeq 2.8$ (see Fig. 6) and the smaller magnitude of the skewness for u and w (see Fig. 5) at $\mu > 0.5$ are also in closer agreement to that observed experimentally in the logarithmic region [4]. However, the eddy shape and the spatial domain used in the present study to produce these results is a representative case, chosen to highlight that sub-Gaussian behavior can be attained for the streamwise velocity simultaneously with super-Gaussian behavior for the spanwise and wall-normal velocity. In fact, we anticipate that a large variety of representative eddy shapes would provide quantitatively similar results, provided the energetic scales increase with distance from the wall, and an exclusion zone (equivalent to μ) is defined during the placement of eddies.

III. CONCLUSIONS

Prior models based on the attached eddy hypothesis, without any restriction on the placement of eddies, have shown good qualitative agreement with experimental data for the mean flow and

the second-order moments of the velocity fluctuations. However, at the fourth-order moment, discrepancies appear between experimental data and the model's results. Specifically, the flatness (kurtosis) of the streamwise velocity fluctuations will invariably be greater than 3, which contrasts with experimental results, which find a streamwise flatness of around 2.8. Our work here demonstrates that this discrepancy can be overcome by mandating a minimum separation between the eddies, when coupled with a physically realistic representative eddy. Such a scenario produces a sub-Gaussian flatness in the streamwise direction, while crucially maintaining a super-Gaussian flatnesses in the spanwise and wall-normal directions. Given the clear similarity to experimental results shown here, we can infer that spatial exclusion between eddies is likely to play an important role in the laws that govern their spatial arrangement. Further, their distributions are likely to be more disperse than a Poisson point process.

---

[1] A. A. Townsend, *The Structure of Turbulent Shear Flow*, 2nd ed. (Cambridge University Press, Cambridge, 1976).

[2] A. E. Perry and M. S. Chong, On the mechanism of wall turbulence, J. Fluid Mech. **119**, 106 (1982).

[3] J. D. Woodcock and I. Marusic, The statistical behaviour of attached eddies, Phys. Fluids **27**, 015104 (2015).

[4] H. H. Fernholz and P. J. Finley, The incompressible zero-pressure-gradient turbulent boundary layer: An assessment of the data, Prog. Aero. Sci. **32**, 245 (1996).

[5] R. J. Adrian, C. D. Meinhart, and C. D. Tomkins, Vortex organization in the outer region of the turbulent boundary layer, J. Fluid Mech. **422**, 1 (2000).

[6] I. Marusic, On the role of large-scale structures in wall turbulence, Phys. Fluids **13**, 735 (2001).

[7] C. D. Tomkins and R. J. Adrian, Spanwise structure and scale growth in turbulent boundary layers, J. Fluid Mech. **490**, 37 (2003).

[8] B. Ganapathisubramani, E. K. Longmire, and I. Marusic, Characteristics of vortex packets in turbulent boundary layers, J. Fluid Mech. **478**, 35 (2003).

[9] C. M. de Silva, N. Hutchins, and I. Marusic, Uniform momentum zones in turbulent boundary layers, J. Fluid Mech. **786**, 309 (2016).

[10] R. Baidya, J. Philip, J. P. Monty, N. Hutchins, and I. Marusic, Comparisons of turbulence stresses from experiments against the attached eddy hypothesis in boundary layers, in *Proceedings of the 19th Australasian Fluid Mechanics Conference* (Australasian Fluid Mechanics Society, Melbourne, 2014).

[11] S. K. Robinson, Coherent motions in the turbulent boundary layer, Annu. Rev. Fluid Mech. **23**, 601 (1991).

[12] J. Zhou, R. J. Adrian, S. Balachandar, and T. Kendall, Mechanisms for generating coherent packets of hairpin vortices in channel flow, J. Fluid Mech. **387**, 353 (1999).

[13] N. Hutchins and I. Marusic, Evidence of very long meandering features in the logarithmic region of turbulent boundary layers, J. Fluid Mech. **579**, 1 (2007).

[14] C. D. Meinhart and R. J. Adrian, On the existence of uniform momentum zones in a turbulent boundary layer, Phys. Fluids **7**, 694 (1995).

[15] A. E. Perry and I. Marusic, A wall-wake model for the turbulence structure of boundary layers. Part 1. Extension of the attached eddy hypothesis, J. Fluid Mech. **298**, 361 (1995).

[16] S. J. Kline, W. C. Reynolds, F. A. Schraub, and P. W. Runstadler, The structure of turbulent boundary layers, J. Fluid Mech. **30**, 741 (1967).

[17] C. Meneveau and I. Marusic, Generalized logarithmic law for high-order moments in turbulent boundary layers, J. Fluid Mech. **719**, R1 (2013).